

Quantum simulation of a general anti- \mathcal{PT} -symmetric Hamiltonian with a trapped ion qubit

Ji Bian,^{1,2,*} Pengfei Lu,^{1,*} Teng Liu,¹ Hao Wu,¹ Xinxin Rao,¹ Kunxu Wang,¹ Qifeng Lao,¹ Yang Liu,^{1,2} Feng Zhu,^{1,2} and Le Luo^{1,2,3,†}

¹*School of Physics and Astronomy, Sun Yat-Sen University, Zhuhai, 519082, China*

²*Center of Quantum Information Technology, Shenzhen Research Institute of Sun Yat-sen University, Shenzhen, 518087, China*

³*State Key Laboratory of Optoelectronic Materials and Technologies, Sun Yat-Sen University (Guangzhou Campus), Guangzhou, 510275, China*

(Dated: March 16, 2022)

Non-Hermitian systems satisfying parity-time (\mathcal{PT}) symmetry have aroused considerable interest owing to their exotic features. Anti- \mathcal{PT} symmetry is an important counterpart of the \mathcal{PT} symmetry, and has been studied in various classical systems. Although a Hamiltonian with anti- \mathcal{PT} symmetry only differs from its \mathcal{PT} -symmetric counterpart in a global $\pm i$ phase, the information and energy exchange between systems and environment are different under them. It is also suggested theoretically that anti- \mathcal{PT} symmetry is a useful concept in the context of quantum information storage with qubits coupled to a bosonic bath. So far, the observation of anti- \mathcal{PT} symmetry in individual quantum systems remains elusive. Here, we implement an anti- \mathcal{PT} -symmetric Hamiltonian of a single qubit in a single trapped ion by a designed microwave and optical control-pulse sequence. We characterize the anti- \mathcal{PT} phase transition by mapping out the eigenvalues at different ratios between coupling strengths and dissipation rates. The full information of the quantum state is also obtained by quantum state tomography. Our work allows quantum simulation of genuine open-system feature of an anti- \mathcal{PT} -symmetric system, which paves the way for utilizing non-Hermitian properties for quantum information processing.

INTRODUCTION

In quantum mechanics, the Hamiltonian of a system is typically taken to be Hermitian in order to generate real eigenenergy spectrum. However, as pointed out by Bender et al. [1], non-Hermitian Hamiltonians obeying parity-time (\mathcal{PT}) symmetry could still give real eigenenergies. \mathcal{PT} -symmetric Hamiltonians exhibit various exotic behaviors, one of which is \mathcal{PT} -symmetry-breaking transitions that show up at an exceptional point (EP). At an EP, the eigenenergies and eigenstates of the Hamiltonian become degenerate [2–7]. Experimental studies on \mathcal{PT} -symmetry in classical systems have stimulated various applications such as lasing [8], optimal energy transfer [9] and enhanced sensing [10], etc. Recently, \mathcal{PT} -symmetric Hamiltonians are also constructed in genuine quantum systems, e.g., ultracold atoms [4], NV-centers [7], trapped ions [5, 6], and superconducting quantum circuits [11], etc. These allow quantum signatures such as perfect quantum coherence at EP to be revealed [5]. Moreover, the topological structure of exceptional points is utilized to realize, e.g., robust quantum control [12].

Not limited to \mathcal{PT} symmetry, EP also appear in systems with anti- \mathcal{PT} symmetry [13–15]. As an important counterpart of the \mathcal{PT} symmetry, anti- \mathcal{PT} symmetry has been studied in various physical systems [16, 17], including coupled waveguides [18], nanophotonics [19], micro-

cavities [20], lossy resonators [21], optical fibres [22], optical systems with atomic media [23, 24], and electrical circuit resonators [13]. An anti- \mathcal{PT} -symmetric Hamiltonian H_{APT} satisfying $\{\mathcal{PT}, H_{\text{APT}}\} = 0$ is related to a \mathcal{PT} -symmetric Hamiltonian H_{PT} by $H_{\text{APT}} = \pm i H_{\text{PT}}$. Here \mathcal{P} and \mathcal{T} denote parity and time reflection operation, $\{\cdot\}$ denotes anticommutator [1]. As a result, properties similar to \mathcal{PT} -symmetric Hamiltonians such as eigenstates coalescing at EP and spontaneous symmetry-breaking transition show up [13]. The information and energy exchange between anti- \mathcal{PT} -symmetric systems and environment are different from the \mathcal{PT} -symmetric counterpart. These result in different information-exchange scheme, e.g., coherence flow [25], between anti- \mathcal{PT} -symmetric systems and the \mathcal{PT} -symmetric counterpart. Interestingly, recent theoretical works [26, 27] studied the evolution of qubits under H_{APT} when coupled to a bosonic bath, and claim that these qubits decohere more slowly compared to those under Hermitian or \mathcal{PT} -symmetric Hamiltonians. This suggests that the anti- \mathcal{PT} -symmetric Hamiltonian as a whole is a useful concept in advancing quantum information processing under decohering environment. Therefore, it is important to carry out further experimental research on the eigensystem structure and environmental energy-exchange scheme of a generic anti- \mathcal{PT} -symmetric system.

So far the experiments on anti- \mathcal{PT} -symmetric Hamiltonian construction are mainly limited to classical systems [13] and ensemble spin systems [28]. Here, we demonstrate the implementation of an individual quantum system acquiring anti- \mathcal{PT} symmetry. We realize the

* These authors contributed equally to this work.

† luole5@mail.sysu.edu.cn

evolution under H_{APT} by designing appropriate pulse sequences, as a standard technique in quantum simulation experiments [29]. The sequence consists of an evolution under a passive \mathcal{PT} -symmetric Hamiltonian H_{M} sandwiching between two $\pi/2$ pulses with opposite phases. The evolution under H_{M} is achieved by a dissipation scheme as demonstrated in [4–6], in the context of \mathcal{PT} -symmetric Hamiltonian construction. We experimentally verify the anti- \mathcal{PT} -symmetric Hamiltonian by studying its anti- \mathcal{PT} phase transition behavior. We obtain the eigenvalues at different coupling strength by preparing a certain initial state, evolving it under H_{APT} for some known duration, and measure the overlap between the evolved state and the initial state, similar to [6]. The results clearly show the transition from anti- \mathcal{PT} symmetry region to anti- \mathcal{PT} symmetry broken region. The full information of the quantum states, i.e., the population as well as the coherence, is also obtained by quantum state tomography. This enables further studies on anti- \mathcal{PT} -symmetric systems, e.g., the information flow [28] and the topological state transfer near an EP [30] to be conducted. Our work could also serve as a first step towards harnessing non-Hermitian \mathcal{PT} or anti- \mathcal{PT} physics to advance the field of quantum information processing [11, 31].

ANTI- \mathcal{PT} -SYMMETRIC HAMILTONIAN CONSTRUCTION

The anti- \mathcal{PT} -symmetric Hamiltonian we want to construct reads

$$H_{\text{APT}} = -2JI_z + 2i\Gamma I_x - i\Gamma \mathbf{I}, \quad (1)$$

where

$$I_x = \frac{1}{2} \begin{pmatrix} 0 & 1 \\ 1 & 0 \end{pmatrix}, \quad I_y = \frac{1}{2} \begin{pmatrix} 0 & -i \\ i & 0 \end{pmatrix}, \quad I_z = \frac{1}{2} \begin{pmatrix} 1 & 0 \\ 0 & -1 \end{pmatrix}$$

are angular momentum operators, and Γ, J are real parameters. Indeed, $\{\text{PT}, H_{\text{APT}}\} = 0$, satisfying the anti- \mathcal{PT} requirement [24], where $\text{P} = 2I_x$, $\text{T} = *$ denotes complex conjugation operation. Given a qubit with eigenstates $|0\rangle = (1, 0)^T$ and $|1\rangle = (0, 1)^T$, H_{APT} in Eq. (1) could be realized as follows.

1) We first realize a passive \mathcal{PT} -symmetric Hamiltonian through a spin-dependent dissipation scheme, which is first realized in cold atoms [4], then in trapped ions [5]. This is achieved by coupling $|0\rangle$ and $|1\rangle$ by a control field (e.g., a microwave field) with coupling strength J , and generate a loss of population on $|1\rangle$ with effective loss rate 4Γ . The population loss could be achieved by adding a dissipative beam [6] as will be explained in the following section. Now we have constructed the passive \mathcal{PT} -symmetric Hamiltonian $H_{\text{M}} = 2i\Gamma I_z + 2JI_x - i\Gamma \mathbf{I}$. 2) We then realize the final anti- \mathcal{PT} -symmetric Hamiltonian (1) by designing appropriate pulse sequences, as is

typically done in quantum simulation experiments [29]. According to the identities

$$Re^A R^\dagger = e^{RAR^\dagger}, \text{ if } RR^\dagger = \mathbf{I}, \quad (2)$$

for arbitrary square matrices A ; and

$$e^{-i\theta I_\alpha} I_\beta e^{i\theta I_\alpha} = I_\beta \cos \theta + I_\gamma \sin \theta, \quad (3)$$

where $\{\alpha, \beta, \gamma\}$ are cyclic permutations of $\{x, y, z\}$, the evolution of the system under (1), $e^{-iH_{\text{APT}}\tau}$, could be realized by sandwiching the evolution under H_{M} between two $\pi/2$ pulses along $\pm y$ axis. That is, denote $R_y(\theta) = e^{-i\theta I_y}$ the rotation along y for θ , then by taking $R = R_y(\pi/2)$ and $A = -iH_{\text{M}}\tau$, we have

$$\begin{aligned} R_y\left(\frac{\pi}{2}\right) e^{-iH_{\text{M}}\tau} R_y\left(-\frac{\pi}{2}\right) &= e^{-iR_y\left(\frac{\pi}{2}\right)H_{\text{M}}R_y\left(-\frac{\pi}{2}\right)\tau} \\ &= e^{-i(2i\Gamma I_x - 2JI_z - i\Gamma \mathbf{I})\tau} = e^{-iH_{\text{APT}}\tau}. \end{aligned}$$

The pulse sequence is illustrated in Fig. 1, (a).

Finally, we obtain the evolution under anti- \mathcal{PT} -symmetric Hamiltonian for time τ . τ equals the evolution time under H_{M} , i.e., the duration of the middle pulse in Fig. 1, (a). One could change the duration of the middle pulse to obtain evolutions under H_{APT} for arbitrary times. It is noted that, a Floquet scheme [6, 32] has used similar pulse sequence, but needs many cycles to generate the desired evolutions.

Starting from $|0\rangle$, without the dissipative beam, the state is fixed during the middle pulse and will return to $|0\rangle$ at the end of the sequence. The addition of dissipation during the middle pulse evolves the state to a different point in the Hilbert space, which essentially result in the evolution of H_{APT} . To better understand the evolution of the quantum state in the Hilbert space under dissipation, we construct a non-Hermitian Bloch sphere using CPT symmetry [33] as illustrated in Fig. 2. The system is evolving under H_{M} during the middle pulse, for such a passive \mathcal{PT} -symmetric non-Hermitian Hamiltonian, a linear operator C exists, which satisfies $[H_{\text{M}}, C] = 0$ and $[\text{PT}, C] = 0$ [33, 34]. Replacing the complex conjugate with the CPT-conjugate, the new inner product for an arbitrary state $|\psi\rangle$ can be written as the form of Dirac inner product [35]: $\langle\psi|\psi\rangle^{\text{CPT}} = \langle\psi|\text{P}^T C^T|\psi\rangle$. The structure of the resulting new Hilbert space (CPT-inner-product space) depends on C , which could be written as $C = 2/\sqrt{1-r^2}(I_x + irI_z)$, where $r := \Gamma/J$. Then, taking the normalized eigenstates $|\epsilon_+\rangle$ and $|\epsilon_-\rangle$ of H_{M} as a basis, an arbitrary state $|\psi\rangle$ could be written as $|\psi\rangle^{\text{CPT}} = R \cos \frac{\Theta}{2} |\epsilon_+\rangle + R \sin \frac{\Theta}{2} e^{i\Phi} |\epsilon_-\rangle$. As $\langle\epsilon_\pm|\epsilon_\pm\rangle^{\text{CPT}} = 1$ and $\langle\epsilon_\pm|\epsilon_\mp\rangle^{\text{CPT}} = 0$, the evolution of $|\psi\rangle$ under H_{M} could be demonstrated on a newly constructed non-Hermitian Bloch sphere with radius R . The axes are chosen such that the point $(x=0, y=0, z=\pm R)$ represents $R|\epsilon_\pm\rangle$, Θ equals the angle spanned by the state vector and z axis, and Φ equals the angle between the state

vector and x axis. As an example, the trajectory under H_M with initial state $|\psi_0\rangle = 1/\sqrt{2}(|0\rangle - |1\rangle)$, $J = 0.06$ MHz, $\tau = 50 \mu\text{s}$, $\Gamma = 0.03$ MHz is plotted on the unit ($R = 1$) non-Hermitian Bloch sphere, as illustrated in Fig. 2, (a). If Γ is changed to 0.12 MHz, while other parameters remain unchanged, the trajectory is plotted on another non-Hermitian Bloch sphere, as shown in Fig. 2, (b). If $\Gamma = 0$, the state is fixed on the sphere. As Γ gets larger, the state starts to evolve and trajectories appear on the corresponding CPT sphere. This helps to better understand the evolution under both Hermitian coupling and non-Hermitian dissipation.

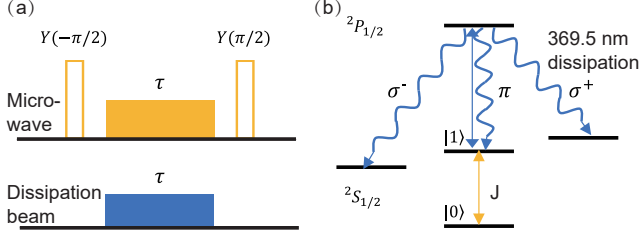


FIG. 1. (color online). (a) The pulse sequence utilizing microwave and dissipative beam to realize H_{APT} . $Y(\pm\pi/2)$ denotes rotation along $\pm y$ axis by $\pi/2$. τ is the duration of the middle pulse which is realized by simultaneous application of microwave and dissipative beam. (b) The trapped $^{171}\text{Yb}^+$ ion as a qubit. The hyperfine states in $^2\text{S}_{1/2}$ with $m = 0$ correspond to qubit levels $|0\rangle$ and $|1\rangle$. The 369.5 nm dissipative beam, the spontaneous decay channel, and the microwave control field with coupling strength J are explained in the main text.

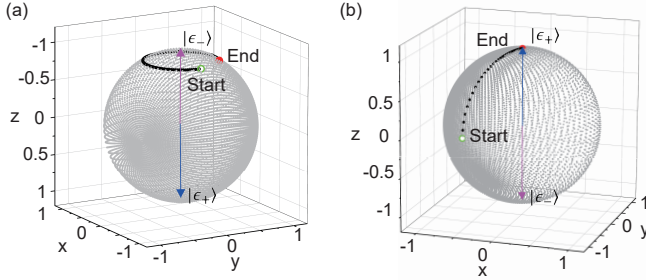


FIG. 2. (color online). Evolution of the state under H_M on the non-Hermitian Bloch sphere. The choice of coordinates are given in the main text. $|\epsilon_{\pm}\rangle$ are marked on the sphere. The state starts from $\frac{1}{\sqrt{2}}(|0\rangle - |1\rangle)$, and evolves under H_M for τ . Here $J = 0.06$ MHz, $\tau = 50 \mu\text{s}$, $\Gamma = 0.03$ MHz in (a) and $\Gamma = 0.12$ MHz in (b).

EXPERIMENTAL IMPLEMENTATION AND VERIFICATION OF THE ANTI- \mathcal{PT} -SYMMETRIC HAMILTONIAN

We conduct the experiment on a trapped $^{171}\text{Yb}^+$ quantum processor. Qubit levels $|0\rangle$ and $|1\rangle$ correspond to the

two hyperfine ground states $|F = 0, m = 0\rangle$ and $|F = 1, m = 0\rangle$, as demonstrated in Fig. 1, (b). The qubit splitting $\omega_{\text{HF}} \approx 12.6$ GHz. The two levels are coupled by microwave fields with coupling strength J . The population loss is realized by a dissipation scheme, as demonstrated in [6]. The ion is excited from $|F = 1, m = 0\rangle$ to $^2\text{P}_{1/2}$ state by a 369.5 nm dissipative beam, which contains only π -polarization components. This ensures that excitations from states $|F = 1, m = \pm 1\rangle$ are forbidden according to selection rules. Through spontaneously emitting σ or π polarized photons, the excited $^2\text{P}_{1/2}$ state will decay to the $|F = 1, m = 0, \pm 1\rangle$ states in the $^2\text{S}_{1/2}$ manifold. This effectively generates a population loss on $|1\rangle$ at a loss rate 4Γ [6]. The whole scheme is illustrated in Fig. 1, (b).

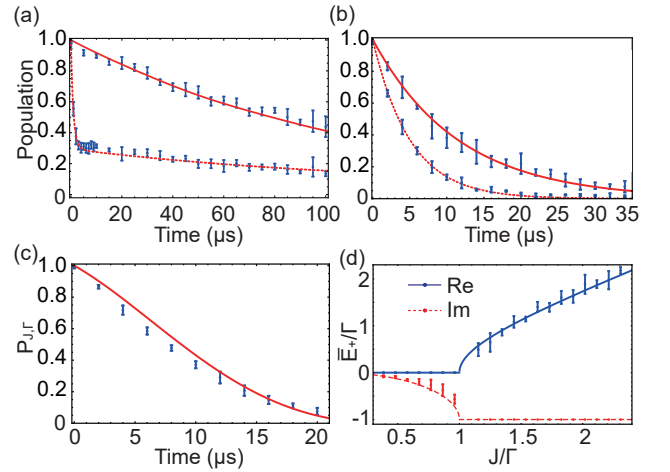


FIG. 3. (color online). (a) shows population on $|0\rangle$ as a function of evolution time, with $J = 0.06$ MHz. Blue dots are experimental data, and the red curve is a fit to ρ_{00} in (4). Γ is fitted to be 0.004 MHz for the solid curve and 0.53 MHz for the dashed curve. Hence the anti- \mathcal{PT} -symmetry is broken (preserved) for the solid curve (dashed curve). (b) shows the evolution of ρ_{11} under pure dissipation. Γ is fitted to be 0.022 (0.050) for the solid (dashed) curve. (c) shows the theoretical $P_{J,\Gamma}(\tau)$ (solid lines) and the measured $P_{J,\Gamma}(\tau)$ (dots), $\Gamma = 0.022$ MHz and $J = 0.065$ MHz. (d) shows the eigenvalue \bar{E}_+ . Dots representing average value of the eigenvalue, together with the error bars, are obtained by repeating the experiment 3 times as explained in the main text. The solid (dashed) curve represents real and imaginary part of the theoretical eigenvalue.

The evolution under H_{APT} is realized by the sequence depicted in Fig. 1, (a): 1) Apply a $\pi/2$ microwave pulse along $-y$ axis in the rotating frame. 2) Apply a microwave field along x axis with strength J and a dissipative beam with dissipation rate 4Γ simultaneously, for a duration τ . This creates an evolution under H_M for τ . 3) Finally, a $\pi/2$ pulse along y is implemented. The resulting whole evolution is $U(\tau) = e^{-iH_{\text{APT}}\tau}$, i.e., an evolution under H_{APT} for time τ . Denote the initial state $|\Psi(0)\rangle$, and the density matrix at time τ , $\rho(\tau) = |\Psi(\tau)\rangle\langle\Psi(\tau)|$, where $|\Psi(\tau)\rangle = e^{-iH_{\text{APT}}\tau}|\Psi(0)\rangle$. Starting from $|0\rangle$, the

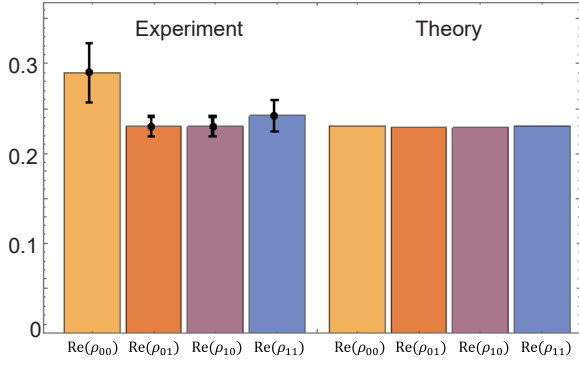


FIG. 4. (color online). Tomography of the density matrix ρ after an evolution under H_{APT} for $10 \mu\text{s}$, with $J/\Gamma \approx 0.15$. The imaginary parts of the density matrix are close to 0 and are not shown.

density matrix elements $\rho_{ij}(\tau) = \langle i|\rho(\tau)|j\rangle$ read

$$\begin{aligned}\rho_{00}(\tau) &= e^{-2\Gamma\tau} \left\{ \cos^2(\tau\sqrt{J^2 - \Gamma^2}) + \left[\frac{J \sin(\tau\sqrt{J^2 - \Gamma^2})}{\sqrt{J^2 - \Gamma^2}} \right]^2 \right\}, \\ \rho_{11}(\tau) &= \frac{e^{-2\Gamma\tau} \Gamma^2 \sin^2(\sqrt{J^2 - \Gamma^2}\tau)}{J^2 - \Gamma^2}, \\ \rho_{01}(\tau) &= e^{-2\Gamma\tau} \Gamma \frac{i \sin(\sqrt{J^2 - \Gamma^2}\tau)}{\sqrt{\Gamma^2 - J^2}} [\cos(\sqrt{J^2 - \Gamma^2}\tau) \\ &\quad + \frac{J \sin(\sqrt{J^2 - \Gamma^2}\tau)}{\sqrt{\Gamma^2 - J^2}}].\end{aligned}\quad (4)$$

$\rho_{00}(\tau)$ is measured for both $J/\Gamma < 1$ and $J/\Gamma > 1$, as shown in Fig. 3, (a). $J = 0.06$ MHz is obtained separately by fitting the Rabi oscillation. Γ could be obtained by fitting according to $\rho_{00}(\tau)$ in (4), e.g., $\Gamma = 0.004$ (0.53) MHz for the solid (dashed) curve. Similarly, $\rho_{11}(\tau)$ and $\rho_{01}(\tau)$ could be obtained by standard quantum state tomography technique. Γ could also be independently calibrated by preparing the system in $|1\rangle$, let it evolve under pure dissipation (the corresponding Hamiltonian is $-2i\Gamma|1\rangle\langle 1|$) for τ , measure the final population on $|1\rangle$ and fit it with $e^{-4\Gamma\tau}$. For example, in Fig. 3, (b), two such processes are plotted and Γ is fitted to be 0.022 (0.050) MHz for the solid (dashed) curve.

To verify the constructed anti- \mathcal{PT} -symmetric system, we experimentally study the anti- \mathcal{PT} phase transition behavior. The eigenvalues E_{\pm} of the anti- \mathcal{PT} -symmetric Hamiltonian (1), or equivalently $\bar{E}_{\pm} = E_{\pm}/\Gamma$, could serve to characterize this transition,

$$\bar{E}_{\pm} = -i \pm \frac{\sqrt{J^2 - \Gamma^2}}{\Gamma}. \quad (5)$$

One way [7] to obtain \bar{E}_{\pm} and verify the constructed system would be calibrating J and Γ independently, and curve fitting $\rho_{00}(\tau)$ to the theoretical predictions. Here we utilize a more effective method to measure the overlap between a certain initial state and the corresponding

evolved state [6], as

$$\begin{aligned}P_{J,\Gamma}(\tau) &= \left| \frac{\langle 0| + i\langle 1|}{\sqrt{2}} \exp(-iH_{\text{APT}}\tau) \frac{|0\rangle - i|1\rangle}{\sqrt{2}} \right|^2 \\ &= \cos^2(\sqrt{J^2 - \Gamma^2}\tau) e^{-2\Gamma\tau},\end{aligned}\quad (6)$$

one could first measure $P_{J,\Gamma}(\tau)$ by preparing the initial state $(|0\rangle - i|1\rangle)/\sqrt{2}$, let it evolve under H_{APT} for a known τ , and measure the overlap between the evolved state and $(|0\rangle - i|1\rangle)/\sqrt{2}$ (left multiply its conjugate transpose). Together with the independently measured Γ , one could obtain $\sqrt{J^2 - \Gamma^2}$ by calculating the arccos or arc-cosh function followed by a division over τ , hence \bar{E}_{\pm} is also obtained.

$P_{J,\Gamma}(\tau)$ could be measured by starting from $|0\rangle$, apply a $R_x(\pi/2)$ pulse, let the system evolve according to $e^{-iH_{\text{APT}}\tau}$, then apply a $R_x(-\pi/2)$ pulse and readout the population on $|0\rangle$. For example, in Fig. 3, (c), we first set $\Gamma = 0.022$ MHz by an independent calibration (Fig.2, (b), solid curve), and $J = 0.065$ MHz, this gives the theoretical curve; then $P_{J,\Gamma}(\tau)$ is measured by the above sequence. The theoretical curve and experimental data are close to each other. The experimental procedure to obtain E_{\pm} at different J/Γ is listed below.

1) Γ and J are first calibrated through independent measurements. This gives us a correspondence between the dissipative beam strength (microwave field strength) and Γ (J). In the following we set the dissipative beam strength corresponding to $\Gamma = 0.050$ MHz (Fig.2, (b), dashed curve), and vary the microwave field strength.

2) The initial state is prepared in $|0\rangle$ by optical pumping. Set the microwave field strength corresponding to J .

3) $P_{J,\Gamma}$ is measured at a certain time τ_0 , here we choose $\tau_0 = 1/J$. At this step, we also separately measure Γ as in Fig.3, (b).

4) Plug $P_{J,\Gamma}$, τ_0 and Γ [obtained in 3)] into (6), we obtain $\sqrt{J^2 - \Gamma^2}$. Plug $\sqrt{J^2 - \Gamma^2}$ and Γ [obtained in 3)] into (5), we obtain \bar{E}_{\pm} .

5) Repeat steps 2) to 4) with varying J , we obtain \bar{E}_{\pm} at different J/Γ . Here J/Γ , i.e., the horizontal axis of Fig. 3, (d), are evaluated by the calibrated values in step 1).

6) Repeat steps 2) to 5) three times to obtain the average and variance of \bar{E}_{\pm} . The result is shown in Fig. 3, (d), where only \bar{E}_+/Γ is plotted. The error bars reflect the fact that there are noises in J , Γ , the constructed evolution under H_{APT} , and the readout process.

The system stays in the anti- \mathcal{PT} symmetry region with purely imaginary eigenvalues when $J/\Gamma < 1$. At EP ($J/\Gamma = 1$), the eigenvalues become degenerate and equals to $-i\Gamma$. The system enters the anti- \mathcal{PT} symmetry broken region when $J/\Gamma > 1$, and the eigenvalues start to have real components. The experimental results agree well with the theoretical calculations, as illustrated in Fig. 3, (d).

The full density matrix of the system is further obtained through quantum state tomography. As an example, Fig. 4 shows the experimental density matrix ρ_{exp} at 10 μs , $J/\Gamma \approx 0.15$, together with the theoretical values ρ_{th} . Applying the state fidelity formula $F = |\text{Tr}(\bar{\rho}_{\text{th}}\bar{\rho}_{\text{exp}})|/\sqrt{\text{Tr}(\bar{\rho}_{\text{th}}^2)\text{Tr}(\bar{\rho}_{\text{exp}}^2)}$, where $\bar{\rho}_{\text{exp}} = \rho_{\text{exp}}/\text{Tr}(\rho_{\text{exp}})$, $\bar{\rho}_{\text{th}} = \rho_{\text{th}}/\text{Tr}(\rho_{\text{th}})$ are experimental and theoretical normalized density matrix [28, 36], the fidelity is calculated to be $97.3\% \pm 1.1\%$. Simulation results suggest that the errors might be caused by noises in the dissipative beam and readout pulses. The experimental results match theoretical predictions, which demonstrates the reliability of the constructed anti- \mathcal{PT} -symmetric system.

While the passive \mathcal{PT} -symmetric Hamiltonian is constructed by the state-dependent dissipation scheme in trapped-ions [5, 6], the anti- \mathcal{PT} -symmetric one has not been directly implemented, due to the difficulties in constructing controllable dissipative-coupling between the two qubit states. Our method effectively implements the anti- \mathcal{PT} -symmetric Hamiltonian through adding two additional pulses, arbitrary evolutions under H_{APT} could thus be simulated. Note that in the experiment, the constructed Hamiltonian is exactly (1), which is anti- \mathcal{PT} -symmetric, there is no need to remove the $i\Gamma\mathbf{I}$ term artificially as is done when simulating \mathcal{PT} -symmetric systems [4–6]. Although H_{APT} and $H_{\text{PT}} = \pm iH_{\text{APT}}$ have similar eigensystem structures, a recent work [25] suggests that they behave differently in the context of coherence flow between the system and environment. When taking the phonon degrees of freedom into account, evolutions under H_{APT} might decohere more slowly than those under H_{PT} , as studied in [27]. This suggests that anti- \mathcal{PT} -symmetry is a useful concept in trapped-ion quantum information processing.

CONCLUSION

To conclude, we have successfully implemented an anti- \mathcal{PT} -symmetric quantum system by a single $^{171}\text{Yb}^+$ ion. By sandwiching an evolution under a passive \mathcal{PT} -symmetric Hamiltonian between two $\pi/2$ pulses with opposite phases, we realize the desired evolution under anti- \mathcal{PT} -symmetric Hamiltonian. We experimentally verify the anti- \mathcal{PT} -symmetric Hamiltonian by studying its anti- \mathcal{PT} -symmetric phase transition behaviour. By preparing a certain initial state, evolving it under H_{APT} , and measuring the overlap between the final state and the initial state, we obtain the eigenvalues at different J/Γ . The transition from anti- \mathcal{PT} symmetry region to anti- \mathcal{PT} symmetry broken region, together with the eigenvalue coalescing, are clearly revealed from the data. The full

information of the quantum states, i.e., the population as well as the coherence, are also obtained by quantum state tomography. The experimental results agree well with theoretical predictions.

Based on the constructed anti- \mathcal{PT} -symmetric Hamiltonian and the versatile quantum-control toolbox trapped ions offer [37, 38], further experimental studies on non-Hermitian physics could be envisioned. For example, the information retrieval [28, 32] and topological state transfer [9, 12] in non-Hermitian quantum systems. Our work also paves the way for harnessing non-Hermitian physics in quantum information-processing applications, e.g., qubits with non-Hermitian \mathcal{PT} or anti- \mathcal{PT} -symmetric Hamiltonians could have superior coherence times compared to Hermitian qubits when coupled to a bosonic bath [26, 27].

Note that after this work is finished, we become aware of a similar experiment done recently by L. Ding et al [32]. They implement a Floquet Hamiltonian requiring multi-cycles of pulses to create anti- \mathcal{PT} -symmetric Hamiltonian by periodically driving a dissipative single trapped ion.

DECLARATION OF COMPETING INTEREST

The authors declare that they have no conflict of interest.

ACKNOWLEDGMENTS

Support come from the Key-Area Research and Development Program of Guangdong Province under Grant No. 2019B030330001, the National Natural Science Foundation of China under Grant No. 11774436, No. 11974434 and No.12074439, the fundamental research funds for the Central Universities (Sun Yat-sen University, 2021qntd28). Le Luo receives support from Guangdong Province Youth Talent Program under Grant No. 2017GC010656, Sun Yat-Sen University Core Technology Development Fund. Yang Liu receives support from Natural Science Foundation of Guangdong Province under Grant 2020A1515011159. Ji Bian receives support from China Postdoctoral Science Foundation under Grant 2021M703768.

-
- [1] Carl M Bender, Stefan Boettcher, and Peter N Meisinger. \mathcal{PT} -symmetric quantum mechanics. *Journal of Mathematical Physics*, 40(5):2201–2229, 1999.
 - [2] Carl M Bender, Dorje C Brody, Hugh F Jones, and Bernhard K Meister. Faster than hermitian quantum mechanics. *Physical Review Letters*, 98(4):040403, 2007.

- [3] Chao Zheng, Liang Hao, and Gui Lu Long. Observation of a fast evolution in a parity-time-symmetric system. *Philosophical Transactions of the Royal Society A: Mathematical, Physical and Engineering Sciences*, 371(1989):20120053, 2013.
- [4] Jiaming Li, Andrew K Harter, Ji Liu, Leonardo de Melo, Yogesh N Joglekar, and Le Luo. Observation of parity-time symmetry breaking transitions in a dissipative floquet system of ultracold atoms. *Nature communications*, 10(1):1–7, 2019.
- [5] Wei-Chen Wang, Yan-Li Zhou, Hui-Lai Zhang, Jie Zhang, Man-Chao Zhang, Yi Xie, Chun-Wang Wu, Ting Chen, Bao-Quan Ou, Wei Wu, et al. Observation of pt-symmetric quantum coherence in a single-ion system. *Physical Review A*, 103(2):L020201, 2021.
- [6] Liangyu Ding, Kaiye Shi, Qiuxin Zhang, Danna Shen, Xiang Zhang, and Wei Zhang. Experimental determination of pt-symmetric exceptional points in a single trapped ion. *Physical Review Letters*, 126(8):083604, 2021.
- [7] Yang Wu, Wenquan Liu, Jianpei Geng, Xingrui Song, Xiangyu Ye, Chang-Kui Duan, Xing Rong, and Jiangfeng Du. Observation of parity-time symmetry breaking in a single-spin system. *Science*, 364(6443):878–880, 2019.
- [8] Hossein Hodaei, Mohammad-Ali Miri, Matthias Heinrich, Demetrios N Christodoulides, and Mercedeh Khajavikhan. Parity-time-symmetric microring lasers. *Science*, 346(6212):975–978, 2014.
- [9] Jörg Doppler, Alexei A Mailybaev, Julian Böhm, Ulrich Kuhl, Adrian Girschik, Florian Libisch, Thomas J Milburn, Peter Rabl, Nimrod Moiseyev, and Stefan Rotter. Dynamically encircling an exceptional point for asymmetric mode switching. *Nature*, 537(7618):76–79, 2016.
- [10] Hossein Hodaei, Absar U Hassan, Steffen Wittek, Hipolito Garcia-Gracia, Ramy El-Ganainy, Demetrios N Christodoulides, and Mercedeh Khajavikhan. Enhanced sensitivity at higher-order exceptional points. *Nature*, 548(7666):187–191, 2017.
- [11] M Naghiloo, M Abbasi, Yogesh N Joglekar, and KW Murch. Quantum state tomography across the exceptional point in a single dissipative qubit. *Nature Physics*, 15(12):1232–1236, 2019.
- [12] Wenquan Liu, Yang Wu, Chang-Kui Duan, Xing Rong, and Jiangfeng Du. Dynamically encircling an exceptional point in a real quantum system. *Physical Review Letters*, 126(17):170506, 2021.
- [13] Youngsun Choi, Choloong Hahn, Jae Woong Yoon, and Seok Ho Song. Observation of an anti-pt-symmetric exceptional point and energy-difference conserving dynamics in electrical circuit resonators. *Nature communications*, 9(1):1–6, 2018.
- [14] Chao Zheng, Jin Tian, Daili Li, Jingwei Wen, Shijie Wei, and Yansong Li. Efficient quantum simulation of an anti-p-pseudo-hermitian two-level system. *Entropy*, 22(8):812, 2020.
- [15] Huilai Zhang, Meiyu Peng, Xun-Wei Xu, and Hui Jing. Anti-symmetric kerr gyroscope. *Chinese Physics B*, 31(1):014215, 2022.
- [16] Ying Li, Yu-Gui Peng, Lei Han, Mohammad-Ali Miri, Wei Li, Meng Xiao, Xue-Feng Zhu, Jianlin Zhao, Andrea Alù, Shanhui Fan, et al. Anti-parity-time symmetry in diffusive systems. *Science*, 364(6436):170–173, 2019.
- [17] Jayakrishnan MP Nair, Debsuvra Mukhopadhyay, and GS Agarwal. Enhanced sensing of weak anharmonicities through coherences in dissipatively coupled anti-pt symmetric systems. *Physical Review Letters*, 126(18):180401, 2021.
- [18] Vladimir V Konotop and Dmitry A Zezyulin. Odd-time reversal p t symmetry induced by an anti-p t-symmetric medium. *Physical review letters*, 120(12):123902, 2018.
- [19] Heng Fan, Jiayang Chen, Zitong Zhao, Jianming Wen, and Yu-Ping Huang. Antiparity-time symmetry in passive nanophotonics. *ACS photonics*, 7(11):3035–3041, 2020.
- [20] Fangxing Zhang, Yaming Feng, Xianfeng Chen, Li Ge, and Wenjie Wan. Synthetic anti-pt symmetry in a single microcavity. *Physical Review Letters*, 124(5):053901, 2020.
- [21] Huilai Zhang, Ran Huang, Sheng-Dian Zhang, Ying Li, Cheng-Wei Qiu, Franco Nori, and Hui Jing. Breaking anti-pt symmetry by spinning a resonator. *Nano Letters*, 20(10):7594–7599, 2020.
- [22] Arik Bergman, Robert Duggan, Kavita Sharma, Moshe Tur, Avi Zadok, and Andrea Alù. Observation of anti-parity-time-symmetry, phase transitions and exceptional points in an optical fibre. *Nature Communications*, 12(1):1–9, 2021.
- [23] Yue Jiang, Yefeng Mei, Ying Zuo, Yanhua Zhai, Jensen Li, Jianming Wen, and Shengwang Du. Anti-parity-time symmetric optical four-wave mixing in cold atoms. *Physical review letters*, 123(19):193604, 2019.
- [24] Peng Peng, Wanxia Cao, Ce Shen, Weizhi Qu, Jianming Wen, Liang Jiang, and Yanhong Xiao. Antiparity-time symmetry with flying atoms. *Nature Physics*, 12(12):1139–1145, 2016.
- [25] Yu-Liang Fang, Jun-Long Zhao, Yu Zhang, Dong-Xu Chen, Qi-Cheng Wu, Yan-Hui Zhou, Chui-Ping Yang, and Franco Nori. Experimental demonstration of coherence flow in pt-and anti-pt-symmetric systems. *Communications Physics*, 4(1):1–6, 2021.
- [26] Bartłomiej Gardas, Sebastian Deffner, and Avadh Saxena. Pt-symmetric slowing down of decoherence. *Physical Review A*, 94(4):040101, 2016.
- [27] Julia Cen and Avadh Saxena. Anti-pt-symmetric qubit: Decoherence and entanglement entropy. *Physical Review A*, 105(2):022404, 2022.
- [28] Jingwei Wen, Guoqing Qin, Chao Zheng, Shijie Wei, Xiangyu Kong, Tao Xin, and Guilu Long. Observation of information flow in the anti-symmetric system with nuclear spins. *npj Quantum Information*, 6(1):1–7, 2020.
- [29] Iulia M Georgescu, Sahel Ashhab, and Franco Nori. Quantum simulation. *Reviews of Modern Physics*, 86(1):153, 2014.
- [30] Xu-Lin Zhang, Tianshu Jiang, and Che Ting Chan. Dynamically encircling an exceptional point in anti-parity-time symmetric systems: asymmetric mode switching for symmetry-broken modes. *Light: Science and Applications*, 8(1):1–9, 2019.
- [31] Ching-Ray Chang, Yeu-Chung Lin, Kuei-Lin Chiu, and Tsung-Wei Huang. The second quantum revolution with quantum computers. *AAPPS Bulletin*, 30(1), 2020.
- [32] Liangyu Ding, Kaiye Shi, Yuxin Wang, Qiuxin Zhang, Chenhao Zhu, Ludan Zhang, Jiaqi Yi, Shuaining Zhang, Xiang Zhang, and Wei Zhang. Information retrieval and eigenstates coalescence in a non-hermitian quantum system with anti-pt symmetry. *arXiv preprint arXiv:2107.12635*, 2021.
- [33] Carl M Bender. Introduction to pt-symmetric quantum theory. *Contemporary physics*, 46(4):277–292, 2005.

- [34] Carl M Bender, Dorje C Brody, and Hugh F Jones. Complex extension of quantum mechanics. *Physical Review Letters*, 89(27):270401, 2002.
- [35] Carl M Bender, Dorje C Brody, and Hugh F Jones. Scalar quantum field theory with a complex cubic interaction. *Physical review letters*, 93(25):251601, 2004.
- [36] Dieter Suter and Gonzalo A Álvarez. Colloquium: Protecting quantum information against environmental noise. *Reviews of Modern Physics*, 88(4):041001, 2016.
- [37] Ming-Zhong Ai, Sai Li, Ran He, Zheng-Yuan Xue, Jin-Ming Cui, Yun-Feng Huang, Chuan-Feng Li, and Guang-Can Guo. Experimental realization of nonadiabatic holonomic single-qubit quantum gates with two dark paths in a trapped ion. *Fundamental Research*, 2021.
- [38] Wei Wu, Ting Zhang, and Ping-Xing Chen. Quantum computing and simulation with trapped ions: On the path to the future. *Fundamental Research*, 1(2):213–216, 2021.